doi:10.1006/jmbi.2000.4283 available online at http://www.idealibrary.com on IDEAL® *J. Mol. Biol.* (2001) **305**, 137–149

JMB

Membrane Binding Motif of the P-type Cardiotoxin

Peter V. Dubovskii, Daria V. Dementieva, Eduard V. Bocharov Yuri N. Utkin and Alexander S. Arseniev*

Shemyakin & Ovchinnikov Institute of Bioorganic Chemistry, Russian Academy of Sciences, 16/10 Miklukho-Maklaya str., V-437 Moscow Russia

Carditoxins (CTXs) from cobra snake venoms, the basic 60-62 residue all-beta sheet polypeptides, are known to bind to and impair the function of cell membranes. To assess the membrane induced conformation and orientation of CTXs, the interaction of the P-type cardiotoxin II from *Naja oxiana* snake venom (CTII) with perdeuterated dodecylphosphocholine (DPC) was studied using ^{1}H-NMR spectroscopy and diffusion measurements. Under conditions where the toxin formed a well-defined complex with DPC, the spatial structure of CTII with respect to the presence of tightly bound water molecules in loop II, was calculated using the torsion angle dynamics program DYANA. The structure was found to be similar, except for subtle changes in the tips of all three loops, to the previously described ''major'' form of CTII in aqueous solution illustrated by the ''*trans*'' configuration of the Val7-Pro8 peptide bond. No ''minor'' form with the ''*cis*'' configuration of the above bond was found in the micelle-bound state. The broadening of the CTII backbone proton signals by 5, 16-doxylstearate relaxation probes, together with modeling based on the spatial structure of CTII, indicated a periphery mode of binding of the toxin molecule to the micelle and revealed its micelle interacting domain. The latter includes a hydrophobic region of CTII within the extremities of loops I and III (residues 5-11, 46-50), the basement of loop II (residues 24-29,31-37) and the belt of polar residues encircling these loops (lysines 4,5,12,23,50, serines 11,46, histidine 31, arginine 36). It is suggested that this structural motif and the mode of binding can be realized during interaction of CTXs with lipid and biological membranes.

Keywords: NMR; P-type cardiotoxin (cytotoxin); dodecylphosphocholine micelle; spatial structure; doxylstearate relaxation probe

**Corresponding author*

Introduction

The lethal action of the venom from a snake of the Elapidae family is known to arise primarily from two types of toxins: short-chain neurotoxins and cardiotoxins (CTXs).[1] These small proteins (molecular mass of ~7 kDa) share homology in spatial structure which is held in position by four disulfide bridges at identical positions in the amino acid sequences. The differences in the toxic activity of these molecules were suggested to stem out from the disparity in the spatial arrangement of hydrophobic and hydrophilic side-chains on the surface of these proteins.[2] Neurotoxins were shown to block nerve transmission by virtue of their binding with high affinity to the nicotinic acetylcholine receptor at the post-synaptic level.[3] CTXs are involved in the depolarization of the excitable membranes and are hypothesized to act on membrane proteins involved in transmission of Na^+ and Ca^{2+} currents.[4] They also induce cell lysis and stimulate the activity of tissue lipases.[5] The lytic activity of CTXs is associated with their binding to and damaging of cell membranes.[6,7] In many respects this activity was similar to one observed for α-helical membrane-lytic peptides, like melittin from bee venom.[8] Therefore, the inter-

Abbreviations used: ROESY, rotating frame Overhauser effect spectroscopy; DQF-COSY, double-quantum-filtered correlated spectroscopy; CTX, cytotoxin; CTII, cytotoxin II; DPC, perdeuterated dodecylphosphocholine; PC, phosphatidylcholine; DPPC, dipalmitoylPC; PFG, pulse field gradient; wtg, water-gate; rmsd, root mean-square deviation; SD, standard deviation; DYANA, dynamics algorithm for NMR applications; doxyl, 4′,4′-dimethyloxazolidine-N-oxyl; NOE, nuclear Overhauser enhancement.

E-mail address of corresponding author: aars@nmr.ru

0022-2836/01/010137–13 $35.00/0

action of CTXs with lipid bilayers has received detailed attention.

CTXs were shown to segregate acidic phospholipid from mixtures with phosphatidylcholine (PC)[9,10], to form complexes with dimiristoylphosphatidic acid,[11] to promote the formation of inverted micellar structure within cardiolipin bilayers,[12] to fuse sphingomyelin vesicles causing an extensive leakage of vesicular contents,[13] and to induce aggregation, permeability and fusion of PC/cardiolipin, PC/phosphatidylserine liposomes.[14] With monolayer technique experiments it was shown that CTXs are able to penetrate phospholipid monolayers formed by either neutral or negatively charged phospholipids, but penetration depends on the surface pressure, i.e. the packing density of the phospholipids.[15] Experimental studies of CTX/lipid interactions have led to the division of cardiotoxins into P and S-types differing by the presence of Pro31 or Ser29 residues, respectively.[16] It was found that both types of CTX interact with anionic phospholipids but only the P-type CTXs bind to zwitterionic lipids. It was suggested that phospholipids and ion channel proteins in cell membranes may serve as a target for P and S-type CTXs, respectively.[16] Alternatively, the possibility of the existence of specific cellular receptors acting through the lock-and-key mechanism for CTXs has also been suggested.[17]

Consideration of the spatial structures of CTX' and surface activity measurements provided further evidence that phospholipids may be a site of CTX action. The toxins were proposed to form complexes with phospholipids due to the interaction of positively charged amino groups of lysine residues with phosphate groups of lipids.[18] It was suggested that CTXs possess a specific phospholipid binding site.[19] The molecular hydrophobicity potential analysis of the homologous CTXs revealed the existence of ''functional'' residues probably involved in the interaction with lipid membranes.[20] However, up to the present time little is known about the spatial structure of CTX when interacting with lipid. Some evidence suggests a conformational change within the CTX molecule upon interaction with membranes,[21] whilst other evidence supports the view that the structure remains the same as in aqueous solution.[22,23]

Although membrane perturbation by CTXs are well documented,[16] the mode of CTX association with lipid membranes remains unknown. Different models of CTX positioning within the lipid bilayer were suggested. The P-type CTXs were proposed to form a hydrophopbic column of 34 Å length which might traverse phosphatidylcholine bilayer or bind it peripherally.[24,25] The penetrating binding mode of CTXs was ascribed to the association of three molecules of CTXs.[26] In the trimer the hydrophilic portion of CTXs is hidden from the interaction with the membrane through toxin/toxin interaction but the three-fingered loop region interacts with the hydrocarbon region of the membrane. The S-type CTXs were postulated to interact with the membrane through only one of the three hydrophobic loops.[22] In an alternative model all three loops were proposed to be inserted into the membrane, loop II crossing the bilayer.[2] This model was elaborated later by taking into account the formation of a double inverted micellar structure by cardiolipin in the presence of CTX.[12]

One way to clarify the mode of CTX association with lipid is to make use of a membrane-mimetic environment, in particularly detergent micelles, which has proved itself as a suitable milieu to study polypeptides in a membrane-like environment.[27] In the ^{1}H-NMR study of the interaction of toxin γ with DPC micelles,[28] a probable site of CTX interaction with membranes was elucidated through the observation of significant chemical shift variations in the three hydrophobic loops. In this work we continue to use the same strategy and have focussed on the spatial structure and location of CTII from *Naja oxiana* in DPC micelles.

CTII belongs to P-type CTXs which were shown to interact with lyso-PC micelles,"[16] PC-monolayers[29] and zwitterionic detergent micelles.[28] However, no data on spatial structure and positioning of CTXs at the lipid/water interface have yet been presented. Here we have determined the CTII spatial structure in the DPC micelle-bound state and the location of CTII molecule within the DPC micelle. Previously this CTX has been studied in aqueous solution[30] and the spatial structures of the two forms (differing by a *cis* (''minor'') and *trans* (''major'') configuration of Val7-Pro8 bond) were determined (pdb entries 1cCB9 and 1CCQ).

Results

Stoichiometry of CTII/DPC micelle complex

The typical manifestation of a polypeptide interaction with detergent micelles, such as a broadening and chemical shift variation of ^{1}H-NMR signals, accompanying the change of peptide/detergent ratio, was observed for CTII/DPC mixtures. Figure 1(a) presents the chemical shift dependence of the Met26 amide proton signal on the detergent/toxin ratio at two temperatures, 30 °C and 45 °C. The higher temperature was desirable to obtain more narrow resonances in the ^{1}H-NMR spectra. However, it was impossible to trace out the chemical shift of the Met26 NH proton of the ''major'' CTII form at the DPC/CTII ratios from 2:1 to ~15:1 due to line-broadening. The observed broadening indicated that the exchange between free and micelle-bound states of the loop II of CTII takes place within a few milliseconds. The Leu9 amide proton exhibited a continuous titration curve (Figure 1(a)), which indicated that the exchange time between ''bound'' and ''free'' states for loop I is faster than for loop II. Signals of the ''minor'' CTII form were gradually diminished following the addition of DPC and disappeared at a DPC/CTII ratio above ~10:1. This implies that the

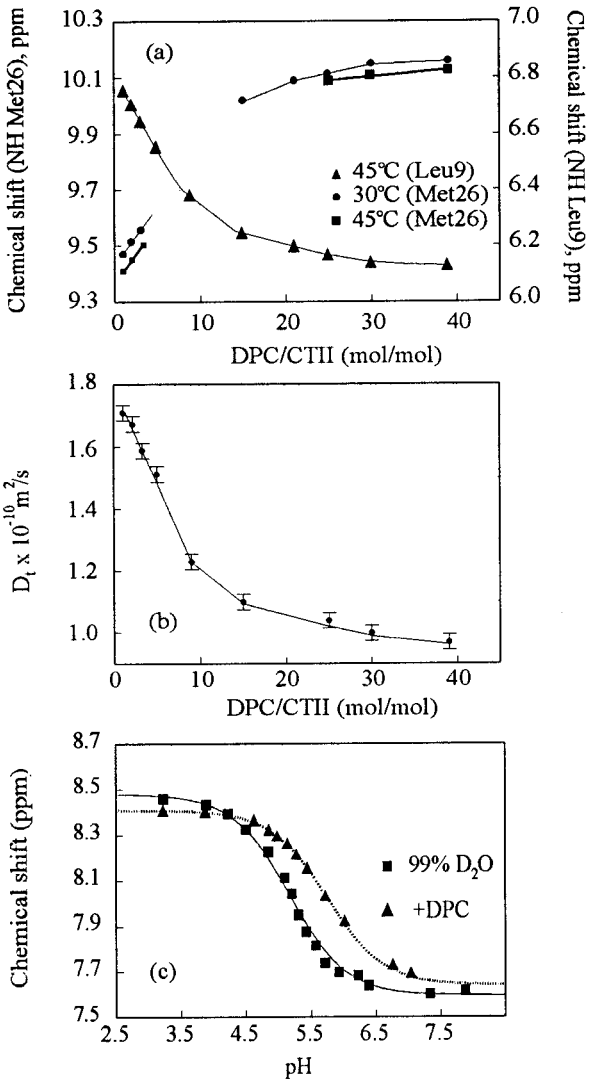

Figure 1. Titration of 3 mM CTII with DPC (pH 5.5). (a) Chemical shifts of the NH proton of Met26 (left vertical axis) at 30, 45 °C and the NH proton of Leu9 at 45 °C (right axis) plotted *versus* the DPC/toxin molar ratio. (b) The translation diffusion coefficient of the CTII molecule plotted *versus* the DPC/CTII molar ratio at 30 °C. Uncertainties are indicated by the vertical bars, (c) pH dependence of the His31 C_2 proton chemical shift of CTII bound to the DPC micelle (1:40, mol/mol) in ^2H_2O (triangles) and in pure ^2H_2O solution (squares) at 30 °C. The continuous lines are the best non-linear fit for the determination of pK_a values.

only ''major'' form of CTII is bound to the micelle (see details below).

The formation of a complex between DPC and CTII was also monitored *via* diffusion measurements at 30 °C (at 45 °C the diffusion measurements were not reliable due to strong convection flows). The dependence of the CTII diffusion constant *versus* DPC/CTII ratio is presented in Figure 1(b). The apparent hydrodynamic radii of the CTII, DPC/CTII complex and DPC micelles, their masses and the aggregation numbers of detergent and CTII molecules, are given in Table 1. These data show that under the conditions used for the structure determination of CTII, approximately two molecules of toxin are bound per one micelle consisting of ~66 molecules of detergent.

Ionogenic state of the His31 residue of CTII in DPC-micelle

The only residue of CTII with an ionogenic side-chain titrating in the physiological pH-range is His31. The additional evidence for a CTII interaction with DPC micelles is given by the change of pK_a value of the imidazole ring of this residue in the micelle-bound state (pK_a ~5.85), compared with aqueous solution (pK_a ~5.25) (Figure 1(c)). The pK_a value of 5.85 falls well into the range of pK_a 4.9 to 6.6 of histidine residues in amphiphilic peptides bound to DPC micelles.[31] The increased pK_a value for the His4 imidazole ring by 0.4 pH unit in CTX A5, due to interaction with lipid micelles, was reported.[29] Such a trend with the larger amplitude of 0.6 pH units was observed for CTII.

Comparison of the CTII proton chemical shifts of micelle-bound state and ''major'' form in aqueous solution

The analysis of NOESY and TOCSY spectra allowed us to obtain nearly complete ^{1}H-NMR assignments of the CTII/DPC complex at 45 °C at pH 5.5. The previously obtained resonance assignments of CTII in aqueous solution at 30 °C, pH 5.0"[32] were extrapolated to 45 °C and pH 5.5 as the NOE pattern shows virtually no change in this pH and temperature range. The chemical shift difference of CTII (''major'' form) protons in aqueous solution and in the DPC micelle bound state (45 °C, pH 5.5) is presented in Figure 2. The most significant differences are confined to amide proton of CTII (residues 4-11, 22-37 and 47-51; Figure 2, middle panel). The side-chain protons experience moderate changes (Figure 2, bottom panel), the peak values being observed for β-proton(s) of residues 7,9,24,34,39 and 50, γ-proton(s) of residues 8,26 and 35, ring-protons of Phe10 and the ε-proton of Arg36 residues. Small changes (within ~0.2ppm) are characteristic for α-proton of CTII residues 5-12, 22-37 and 48-51 (Figure 2, upper panel). Overall, the data of Figure 2 imply that interaction of CTII with the DPC micelle is confined to three regions of CTII: 4-12, 22-39 and 47-50 residues. Interestingly, almost identical regions of toxin γ showed maximal variation of chemical shifts upon interaction with DPC micelles.[28]

Spatial structure of micelle-bound CTII

Although under the conditions used in the present study, approximately two CTII molecules were bound to one DPC micelle (Table 1), no inter-

Table 1. NMR diffusion data of CTII, non-deuterated DPC, and DPC/CTII complex in a $H_2O/^2H_2O$ (6:1) mixture (30 °C, pH 5.5).

Sample	Diffusion constant, ($\times 10^{-10}$ m^2/s)	Apparent hydrodynamic radius, (Å)	Particle mass, ($\times 10^3$Da[a])	Aggregation number
3 mM CTII	1.71 ± 0.03	16.2 ± 0.3	6.6	1
85 mM non-deuterated DPC	1.20 ± 0.02	23.1 ± 0.4	19 ± 2	55 ± 6
120 mM DPC/3 mM CTII	0.97 ± 0.02	28.6 ± 0.6	36 ± 4	66 ± 10/2 ± 0.5

[a] All particle masses were scaled to the molecular mass of CTII through the Stokes-Einstein relationship. No hydration water was taken into account and the density in all particles was assumed to be the same.

molecular NOE contacts between CTIIs were detected. Thus, the spatial structure of CTII in DPC micelles was calculated using the same strategy as for the CTII monomer in an aqueous environment."[30]

The distance constraints used for the structure calculation were assembled from disulfide bridge, hydrogen bond and interproton NOE constraints. The disulfide bridges in the CTII molecule were determined previously[32] and the respective distance constraints were taken without modification. Sequential NOE connectivities together with the hydrogen-deuterium exchange and the spin-spin coupling constant data are presented in Figure 3. The torsion angle constraints were obtained from $^3J_{N\alpha}$, $^3J_{\alpha\beta}$ coupling constants, sequential and intraresidual NOE distance constraints and stereospecific assignments for methylene protons. The location of β-strands, together with data on slowly exchanging amide protons and inter-strand NOEs, resulted in the identification of the 12 hydrogen bonds H^N-O^C:

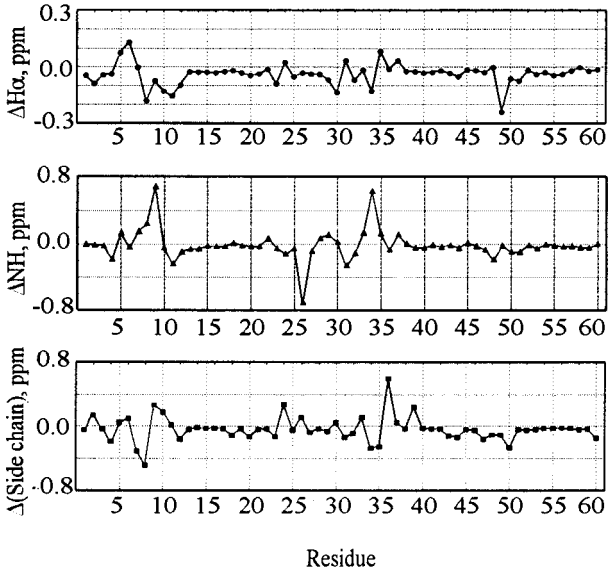

Figure 2. Differences between chemical shifts of CTII (''major'' form) in aqueous solution and of CTII in the DPC micelle (DPC/CTII molar ratio 40:1 (pH 5.5), 45 °C) for α (upper panel) and NH (or δ-protons for Pro-residues) (middle panel) protons, and highest chemical shift variation of side-chain protons (lower panel).

20-39, 21-54, 22-37, 23-52, 24-35, 25-50, 27-48, 35-24, 39-20, 50-25, 52-23 and 58-2. After initial DYANA runs, additional hydrogen bonds were identified: being not constrained in DYANA calculations these hydrogen bonds were found in more than 10 from 20 best structures. The hydrogen bonds which were supported by NOEs, were taken into account in successive DYANA runs. The bound water-protein contacts were detected in ROESY spectra collected at 20 °C and 45 °C (data not shown). Two tightly bound water molecules (one is hydrogen bonded to an NH proton of the Met26 residue, another one is spatially close to δ-protons of the Pro30 residue) were included into the spatial structure calculation protocol as described.[30]

The structural statistics for a CTII/DPC micelle complex (Table 2) shows that the CTII structure is well defined by NMR data, as indicated by the low value of the target function and rmsd values. The stereo view of 20 calculated structures with tightly bound water molecules is presented in Figure 4(a). Clear differences between the spatial structure of the ''major'' form in aqueous solution and the DPC-bound CTII are present in the loop II region (Figure 4(c)), while loops I and III (Figure 4(a) and (d)) are characterized by subtle differences deduced from comparison of backbone and side-chain torsion angles (Figure 5).

Effect of 5 and 16-doxylstearates on the ^{1}H-NMR signals of micelle-bound CTII

Relaxation probes are widely used to determine micelle-embedded[33,34] or water-exposed[35] fragments of polypeptides. In order to elucidate the location of CTII in DPC micelles, stearate was added, spin-labeled at the 5 or 16-position with a doxyl group containing a stable nitroxide radical. The 5 and 16-doxylstearate relaxation probes incorporate into DPC micelle with the nitroxide moiety being preferentially located close to the micelle surface and center, respectively.[33] These probes, in combination, induce broadening of signals of a peptide immersed in any region of the micelle.[36]

The specific broadening of proton signals in the CTII/DPC complex was monitored using TOCSY spectra at the DPC/probe molar ratio of 60:1 (i.e. ca. one relaxation probe per micelle) (Figure 6). To characterize quantitatively the effect of the relaxation probes on the CTII proton, NH/H^{α}

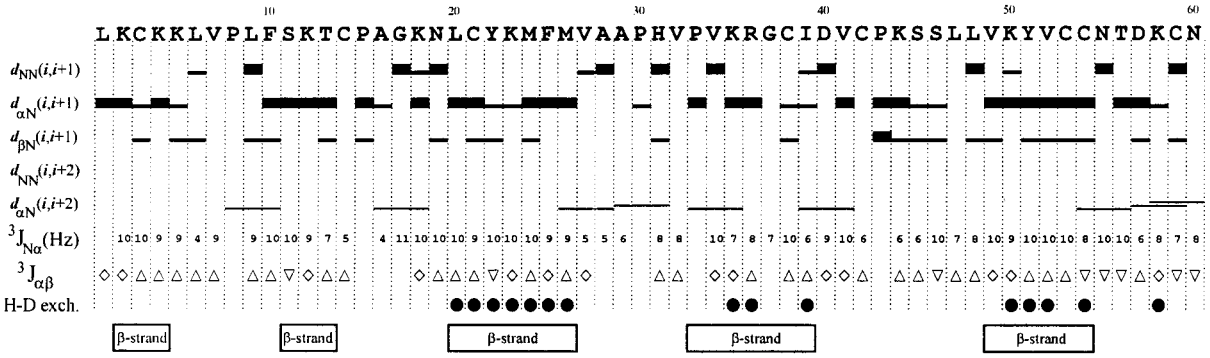

Figure 3. Overview of NMR data defining the CTII spatial structure in the DPC micelle bound state (DPC/CT molar ratio 40:1 (pH 5.5), 45 °C). NOE connectivities are designated as usual: $d_{AB}(i,j)$ is the connection between A and B proton types located in residues i and j, respectively. N, α, β denote the amide, H^{α} and H^{β} protons, respectively. The widths of the bars correspond to the relative intensity of cross-peak in the 100 ms NOESY spectrum. $^3J_{\alpha\beta}$ coupling constants designated by the symbol (Δ) correspond to $J_{\alpha\beta} > 10$ Hz (Val, Thr and Ile residues) or $J_{\alpha\beta a} < 5$ Hz, $J_{\alpha\beta b} > 10$ Hz (other residues), (∇) $J_{\alpha\beta} < 5$ Hz (Val, Thr and Ile residues) or $J_{\alpha\beta a}$, $J_{\alpha\beta b} < 5$ Hz (other residues), and (◇) 5 Hz < $J_{\alpha\beta}$ <10 Hz (Val, Thr and Ile residues) or 5 Hz < $J_{\alpha\beta a}$, $J_{\alpha\beta b}$ < 10 Hz (other residues). The H-^{2}H exchange at 30 °C, symbols (●) denote times of half-exchange of amide protons > ten hours. The sequence of CTII is shown at the top and the location of β-strands at the bottom.

cross-peak amplitudes in the TOCSY spectra of the CTII/DPC complex in the presence and the absence of the probe, were compared. Taken into account attenuation induced by 5- and 16-doxyl-stearates (Figure 7(a)), two groups of cross-peaks can be recognized. The cross-peaks which are unaffected by the probes, i.e. showing a slight if any attenuation in the residual amplitude of NH/H^{α} cross-peaks (1.0(±0.1)), belong to the first group. Amplitudes of another group of NH/H^{α} cross-peaks are strongly attenuated in the presence of the relaxation probes (i.e. with residual amplitudes below the level of ca. 0.8 marked with the continuous line in Figure 7(a)). These residues (5-11, 25-37 and 47-50) reside in the tips of the three loops of CTII. Thus, the use of both relaxation probes reveals a micelle-interacting and non-interacting portion of CTII.

Let us define a micelle surface (or micelle/water interface) around CTII as one dividing CTII into micelle-interacting and non-interacting parts, where the interaction is understood as the broadening of the CTII proton signals by the relaxation probes (Figure 7(a)). Further we assume that: (1) the micelle/water interface can be approximated by a concave or convex sphere (for the sake of simplicity); (2) NH and/or H^{α}-protons corresponding to cross-peaks which are strongly attenuated by the relaxation probe(s) (Figure 7(a), below the continuous horizontal line) are buried beneath the micelle-water interface; (3) NH and H^{α}-protons corresponding to cross-peaks which are not influenced by the relaxation probes (cross-peaks with the

Table 2. Input data for the spatial structure calculation of CTII bound to the DPC micelle and characteristics of the 20 best DYANA structures (mean value ± SD)

Parameter	Units	Quantity	Value
Target function	Å^2		0.11±0.01
No. of distance constraints		NOE	368/0
(upper/lower)		H-bond	112/112
		S-S bridge	12/12
No. of dihedral constraints		Dihedral angle	154
Upper constraint violations		no. > 0.2 Å	0±0
	Å	Maximum	0.11±0.02
	Å	Sum	0.4±0.1
Lower constraint violations		No. > 0.2 Å	0±0
	Å	Maximum	0.04±0.01
	Å	Sum	0.10±0.03
van der Waals constraint violations	Å	Maximum	0.08±0.01
	Å	Sum	0.8±0.1
Dihedral constraint violations	deg.	Maximum	0.5±0.3
	deg.	Sum	0.9±0.8
rmsd of residues 1-60	Å	Backbone	0.57±0.15
	Å	All heavy atoms	1.11±0.13

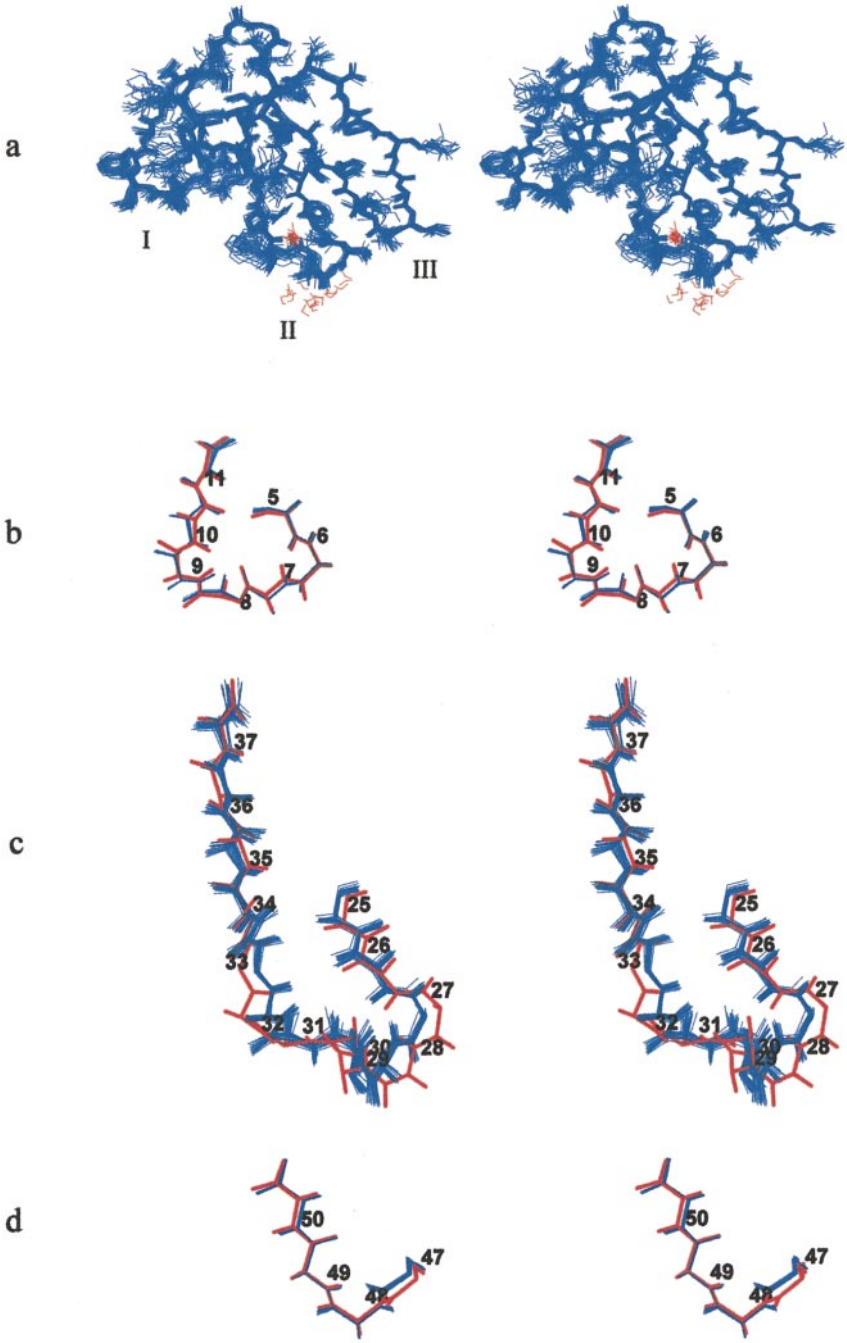

Figure 4. Stereo view of CTII bound to a DPC micelle (a) and structural elements involved into the interaction with the micelle ((b), (c) and (d)). (a) Heavy atom representation of the 20 best DYANA structures of CTII superimposed over backbone atoms of 1-60 residues with tightly bound water molecules shown in red. The three main loops are numbered. Backbone atoms of residues 5-11 (b), 25-37 (c), and 47-50 (d) of CTII superimposed on the respective atoms of the structure number 7 (in red, closest to the mean structure) from the set of 20 structures of CTII in aqueous solution (pdb entry code 1CB9).

residual amplitudes above the horizontal line in Figure 7, (a)) belong to the portion of CTII exposed outside of the micelle.

To select the radius of a sphere dividing the CTII molecule in the micelle-interacting and non-interacting parts we used the same program (DYANA) as in CTII structure calculation (see details in Materials and Methods). The DYANA runs with 40 upper (lower) and 64 lower (upper) distance constraints for convex (concave) spherical surfaces (Figure 8(a)), with the radii in the range 20 Å to 300 Å, resulted in a single solution (characterized by the target function) for each value of the radius (Figure 8(b)). The decreased value of the target function with respect to the radius for the convex sphere, was monotonous (Figure 8(b) squares), whilst for the concave sphere the minimum was observed (Figure 8(b), triangles). The global minimum of the target function of 1.72 $Å^2$ is found for the concave sphere of 71.0(±0.5) Å radius. No significant (>0.9 Å) violation of the distance constraints were found in this case. The model of CTII, corresponding to this solution, is presented in Figure 9. The residues involved in the CTII/micelle interaction, 5-11, 46-50 and 24-29, 31-37 belong to the extremities of loops I and III and to the base of loop II, respectively. These regions also experience

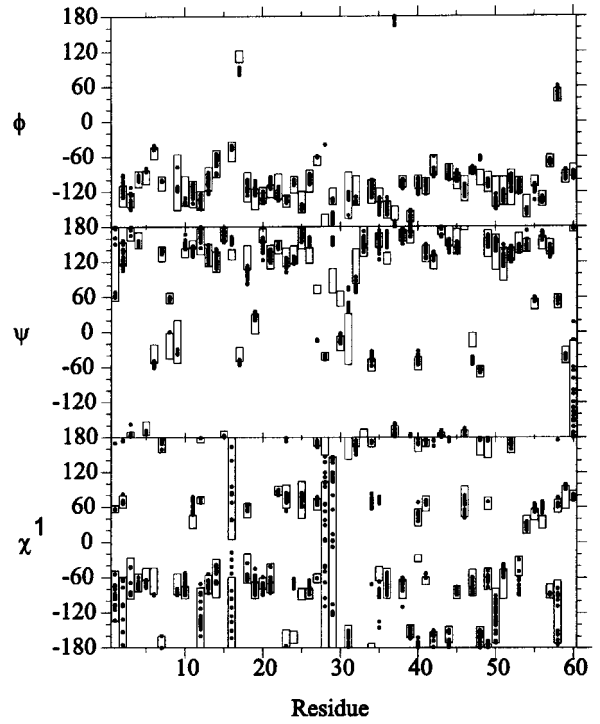

Figure 5. Scatter plots of ϕ, ψ, χ^1 angles for the 20 best DYANA structures of CTII bound to a DPC micelle. The ranges of the corresponding angles for the ''major'' form of CTII in aqueous solution are indicated by the bounding rectangles.

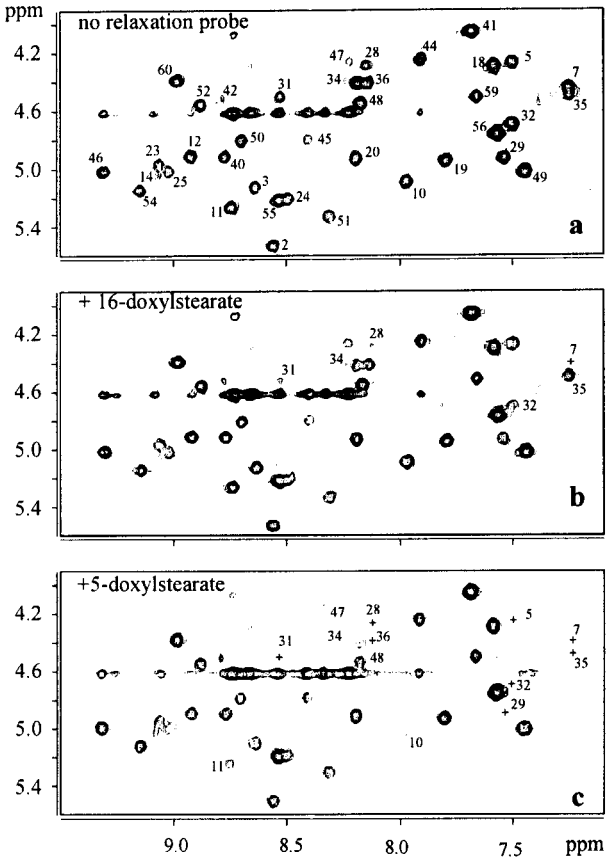

Figure 6. Fragment of the finger-print region of the TOCSY spectrum (60 ms mixing time) of the CTII/DPC complex (molar ratio 1:40 (pH 5.5), 45 °C) without (a) and in the presence of 16-doxylstearate (b) or 5-doxylstearate (c) (DPC/16(5)-doxylstearate = 60:1, mol/mol). Cross-peaks are marked by residue number. In the spectra in (b) and (c) only cross-peaks which were attenuated by more than 50 % of the amplitude are marked. Positions of broadened beyond detection cross-peaks are shown by crosses.

significant variation of proton chemical shifts upon CTII binding to DPC micelles (Figure 2).

The surface of the DPC micelle around CTII molecules is the result of the interaction of CTII with the micelle and is in accordance with the notion that polypeptides may influence shape of a detergent micelle.[36] In particular, as a possible source of distortion of the micelle surface the electrostatic interaction between positively charged NH_3^+ groups of a protein and negatively charged moiety(ies) of a detergent has been suggested.[36]

Discussion

Conformation of the *micelle-bound CTII*

The study of the CTII structure in aqueous solution previously revealed two forms with different configurations of the Val7-Pro8 peptide bond[30]. In the micelle-bound state only CTII with the *''trans''*-configuration of the Val7-Pro8 bond is present. Let us compare the so-called ''major'' form of CTII in aqueous solution (with the *''trans''* configuration of Val7-Pro8 peptide bond; pdb code 1CB9) with the structure of CTII in the DPC micelle (pdb code 1FFJ). CTII molecules in both environments are represented by two antiparallel β-sheets (Figures 3 and 4). The one encompassing loop I consists of two β-strands: within residues 1-5 and 10-14. Another β-sheet includes three β-strands formed by residues 20-26 and 35-39 within loop II and residues 49-55 from loop III. The bend regions connecting β-strands are comprised of residues 6-9, 15-19, 27-34 and 40-48. The extremities of the three fingers of the CTII molecule interact with the DPC micelle and may, potentially be a region of conformational changes. The comparison of backbone angles of CTII in two environments (Figure 5) reveal that this is the case.

The conformation of the 6-9 region was not defined uniquely in aqueous solution.[30] Two distinct clusters of ϕ angles of Leu9 and Phe10 residues and ψ angles of Pro8 and Leu9 were detected. These clusters correspond to different hydrogen bonding: Leu9 NH ... O═C Val7 (γ-turn within residues 7-9) or Phe10 NH ... O═C Val7 (type I β-turn within residues 7-10). In the micelle-bound state in all the best 20 conformers, the

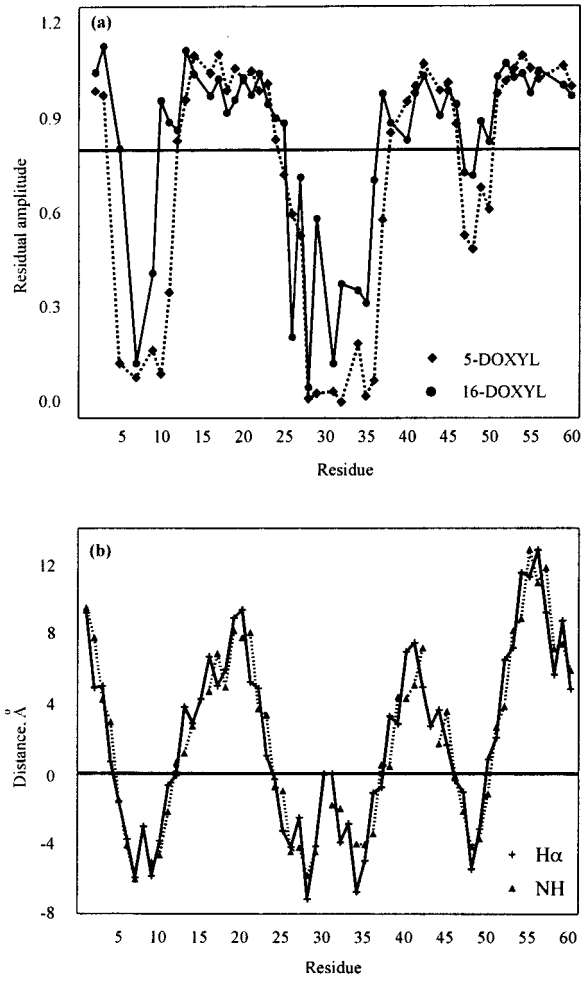

Figure 7. (a) Attenuation of NH/H^{α} cross-peak amplitudes in the finger-print region of the TOCSY (mixing time of 60 ms) spectrum of the CTII/DPC complex (molar ratio 1:40 (pH 5.5), 45 °C) in the presence of 5 (diamonds) or 16-doxylstearate (circles) at the DPC/relaxation probe molar ratio of 60:1. The low-intensity cross-peaks of Lys4, Leu6, Ile39, Asp57 and Lys58 along with Pro-residues were omitted from the analysis. The scatter in the attenuation values is within ±0.1. The horizontal line marks the attenuation level below of which NH/H^{α} cross-peaks are judged to be influenced by the relaxation probes. (b) Distances from NH (triangles) and H^{α} (crosses) protons of a given residue to the micelle/water interface (corresponds to the level of 0 Å marked with the continuous line) approximated as the concave sphere of 71 Å radius. The negative and positive distances correspond to the micelle-embedded and exposed atoms of CTII, respectively.

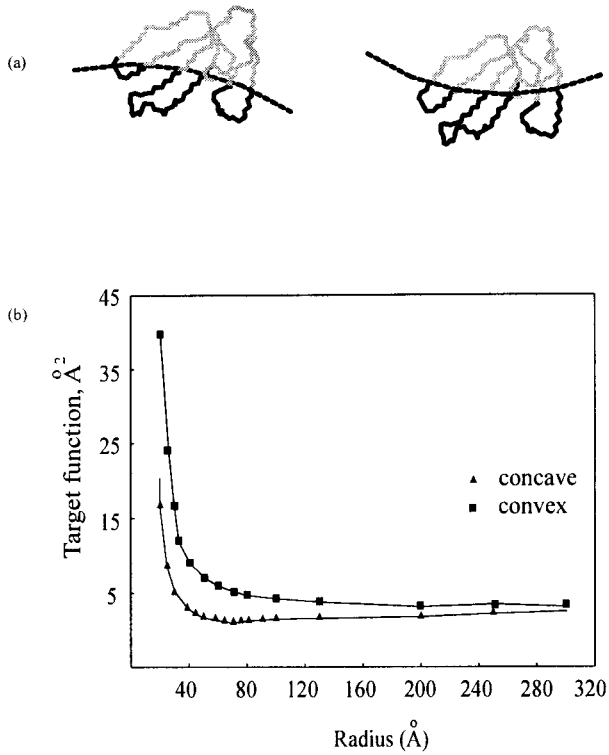

Figure 8. (a) Dissection of CTII into micelle-interacting (thick black line) and non-interacting (gray line) parts with convex (left) or concave (right) surfaces (dotted line). (b) Dependence of the DYANA target function on the radius of the convex (squares) and concave (triangles) micelle/water interface around CTII. The curves are drawn to guide the reader only.

hydrogen bond Leu9 NH ... O═C Val7 is present and thus the conformation of residues 7-9 may be described uniquely as the γ-turn type (Figure 4(b)).

The hydrogen bonding pattern within the 27-34 region of CTII in aqueous solution and in the DPC micelle bound state remain the same: the type II β-turn within residues 26-29 stabilized by the hydrogen bond Ala29 NH ... O═C Met 26 and a β-bulge within residues 24,34 and 35 with bifurcated hydrogen bond Val34 NH/Lys35 NH ... O═C Met 24.[30] The sites of tightly bound water molecules also remain within loop II. One water molecule is hydrogen-bonded to Met26 NH thus drawing apart the two strands of loop II and making the tip of this loop more flat. Another water molecule is found near the δ-protons of the Pro30 residue and its role is not clear. The notable changes in ϕ, ψ angles between the two environments are found in residues 27-31 (Figure 5).

Residues 47-50 at the tip of loop III of CTII interact with the micelle. The conformation of the tip of this loop, formed by residues 46-49, was described as a type I β-turn for CTII in aqueous solution. In addition, non-typical hydrogen bonds for β-turns were detected: Ser46 NH ... O═C Val49, Val49 NH ... O^{γ}-C^{β} Ser 46, Leu48 NH ... O^{γ}-C^{β} Ser46. The latter two hydrogen bonds were not found in the micelle-bound CTII. The backbone angle ϕ of residue Leu48 exhibits a tendency to increase but the ψ angle of Leu47 decreases in the micelle-bound CTII. This results in the rotation of the plane of the Leu47-Leu48 peptide bond (Figures 4(d) and 5).

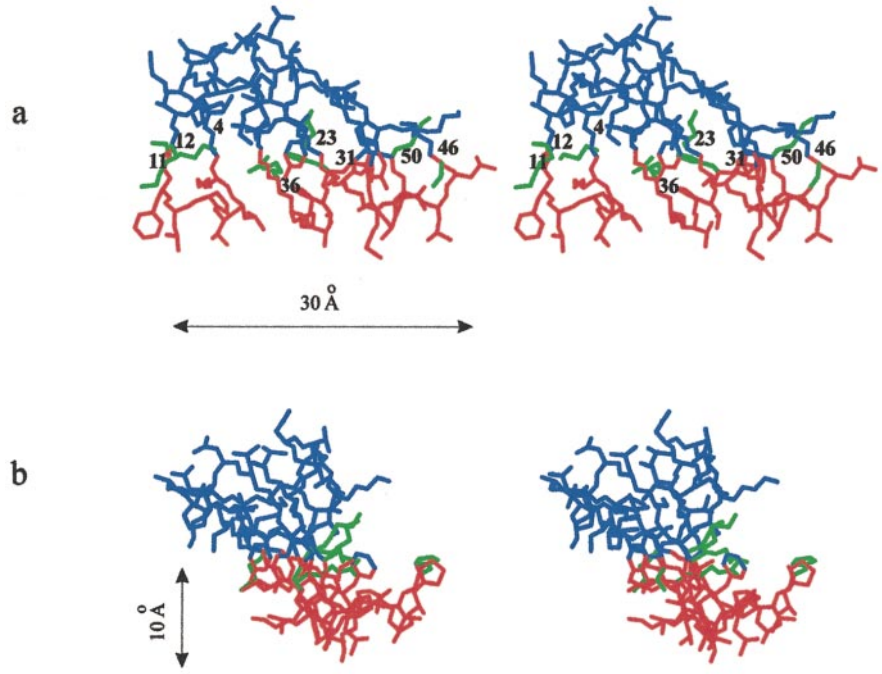

Figure 9. Stereo view of the CTII molecule (all heavy atoms) representation onto the micelle/water interface approximated as a concave sphere of 71 Å radius: front (a) and side-view (b). The CTII part lying beneath the micelle/water interface is shown in red. Polar side-chains (numbered residues) at the micelle/water interface are shown in green. The water-exposed part of CTII is shown in blue.

Residues 4-12, 22-39 and 47-50 at the tips of three CTII fingers constitute regions of maximal chemical shift variation upon toxin binding to DPC micelles (Figure 2). Apparently, this is a result of environmental (Figure 7(b)) and conformational (see Figure 4 and 5) changes associated with the penetration of these residues in the micelle (Figure 9).

Cis versus trans configuration of the Val7-Pro8 bond

Here the structure of micelle-bound CTII was found to be similar to the ''major'' form of CTII in aqueous solution, with the Val7-Pro8 peptide bond in the *trans* configuration.[30] No ''minor'' form having the *cis*-configuration of the bond was found in the micelle-bound toxin. The difference in the binding affinities of these forms to DPC micelles is a result of their structural differences. Inspection of the spatial structures of both of these forms (pdb entries 1CB9 and 1CCQ) shows substantial differences in the shape of loop I. In the major (and in the DPC micelle-bound CTII) form, the tip of this loop, composed of residues 6-10, is flat and the side-chains of Leu6, Val7, Leu9 and Phe10 point approximately in the same direction. In the minor form, the side-chains of Leu6, Val7 and Leu9, Phe10 point in opposite directions. This influences substantially the binding of CTII molecules to DPC micelles.

Model of the CTII/DPC micelle complex

As seen from the data shown in Figure 8, the micelle surface around CTII is best approximated by the concave sphere of ~70 Å radius. This value is far from the Stokes radius of ~ 25 Å of the micelle consisting of ~ 66 detergent molecules. Such a difference implies that the DPC micelle, whose shape in the absence of peptides is best characterized as an ellipsoid,[37] is distorted by the CTII molecule(s).

The position of CTII relative to the interface is in good agreement with the consideration of the sites of the conformational changes within CTII (Figures 4 and 5) or chemical shift variation of CTII protons (Figure 2) upon interaction with the micelle. It is of note that the experimental error (±0.1) in the choice of the residual amplitude according to which CTII molecule is divided into micelle-interacting and non-interacting parts (Figure 7(a)), does not influence the conclusion on the micelle-interacting motif of CTII. This error results in the possible displacement of a CTII molecule as a whole by ±2 Å (Figure 7(b)) relative to the surface, corresponding to the attenuation level of 0.8 (Figure 7(a), continuous horizontal line). The close positioning of CTII to the surface of the micelle (Figure 7(b)) agrees with the profiles of the relaxation-probe induced broadening of backbone cross-peaks (Figure 7(a)). In accordance with its closer disposition to the micelle surface[33] the 5-doxylstearate relaxation probe induces stronger

attenuation compared to the 16-doxylstearate, for the majority of residues (Figure 7(a)). Within each of the I-III loops of CTII the deepening of backbone H^{α} and NH protons (Figure 7(b)) is correlated, with the exception of residues 31-35 of loop II, with the attenuation of the corresponding cross-peaks in TOCSY spectra (Figure 7(a)). However, when one compares attenuation and deepening between the loops of CTII, the loop III region is noteworthy: the deepening of the tip of this loop is comparable to that of loops I and II (Figure 7(b)), but only a small attenuation in the loop III region is observed (Figure 7(a)). There may be several reasons for these contradictions, e.g. difference in accessibility of the backbone atoms to relaxation probes or a deviation of the micelle surface from the simple spherical shape assumed here.

The estimate shows that ~60 % of the surface of CTII is involved in the interaction with the micelle. The micelle-interacting domain of CTII has clear amphiphilic structure. It is formed by residues 5-11, 46-50 and 24-29, 31-37 (whose backbone H^{α} or/and NH atoms are beneath the micelle surface, i.e. below the 0 Å level; Figure 7(b)), residing at the extremities of loops I and III and at the base of loop II, respectively. Although not used directly in the calculations the side-chains of CTII adopted a characteristic positioning with reference to the micelle surface (Figure 9). The hydrophobic side-chains of residues Leu6, Val7, Pro8, Leu9, Phe10, Met26, Val27, Ala28, Ala29, Pro30, Val32, Pro33, Val34, Leu47, Leu48 and Val49 form a continuous hydrophobic belt spreading from the tip of loop I to the tip of loop III, with a length of ~ 30 Å. The width of this domain is ~ 10 Å (Figure 9). The side-chains of the polar residues Lys4, Lys5, Ser11, Lys12, Lys23, His31, Arg36, Ser46 and Lys50 (whose H^{α} and NH atoms are within ±2 Å of the micelle surface; Figure 7(b) and Figure 9, in green), are at the top of the micelle-penetrating domain of CTII. Thus, the polar groups of the side-chains of Lys, Ser and His residues at the borders of CTII loops are found near the micelle/water interface. This is also the case for the Lys35 residue although its backbone atoms are ~ 5 Å beneath the micelle interface (Figure 7(b)). According to the snorkel hypothesis[38], the amphipathic character of lysine residues causes them to extend into the aqueous interfacial solution so that its non-polar van der Waals surface can contact the hydrophobic core of a membrane. From the other point of view, the lysine side-chains of membrane proteins prefer to be in contact with phosphate moities of phospholipids[39]. The positioning of lysine residues encircling loops I-III of CTII in the DPC micelle conforms to these rules.

The present study shows that upon binding of the P-type CTX to a DPC micelle, all three I-III loops are involved in the interaction. Most probably, this peripheral mode of binding remains effective in the case of phospholipid membranes. This conclusion is supported by the consideration of the geometry and amphiphilic properties of the micelle-interacting motif of CTII (see above). Taking into account that the polar part (the region of the membrane encompassing phosphate, glycerol and carbonyl groups of lipid molecules) of the hydrated PC bilayer constitutes about 7-12 Å,[40] CTII can span this region, penetrating into the hydrophobic core of the bilayer with the side-chains of its hydrophobic stretch, leaving charged groups of the residues of its polar belt near the lipid/water interface. This disposition of CTII in the lipid bilayer is in accordance with ^{2}H, ^{31}P-NMR data on the conformational and dynamic states of the phosphocholine head group of DPPC, segmental order parameters at the carbon atoms of the acyl chain of lipid molecules showing that the P-type CTX A3 interacts with DPPC peripherally.[25] Therefore, we presume that the peripheral mode of the association of CTII with DPC micelles is applicable to phospholipid bilayers and biological membranes.

Materials and Methods

Sample preparation

CTII was prepared according to the previously described methods.[32] Non-deuterated dodecylphosphocholine and the perdeuterated analog was prepared as described.[41] 5 and 16-doxylstearates were products of Sigma (St. Louis, the Missouri). $^{2}H_2O$, $C^{2}H_3O^{2}H$ (99.9 %) were purchased from ISOTOPE (Russian Federation).

The sample was prepared by dissolving CTII (10 mg) in 0.55 ml of a $H_2O/^{2}H_2O$ (6:1, v/v) mixture and then the required amount of DPC was added stepwise from the 240 mM stock solution (in $H_2O/^{2}H_2O$, 6:1). The pH of the sample was adjusted with diluted KOH, HCl and was kept at pH 5.5 in all experiments for structure determination and in the study based on the use of the relaxation probes. For the elucidation of the pK_a values of ionogenic groups of CTII titrating in the physiological pH range, the pH of the samples (CTII or CTII/DPC in 99.9 % $^{2}H_2O$ solution) was varied in the range pH 3 to 8. pH values are given as the direct pH meter reading. After the NMR spectra required for characterization of CTII structure and stoichiometry of CTII/DPC complex were measured, the sample was liophilized and dissolved in $^{2}H_2O$ for the measurement of deuterium exchange rates of amide protons. The freshly prepared samples of CTII (5 mg) and appropriate amounts of DPC (to keep the molar ratio of CTII/DPC = 1:40 as in the structural study) in 0.55 ml of $H_2O/^{2}H_2O$ (6:1) were used for the titration with 5 and 16-doxylstearates. The spin-probes were added as a solution in methanol-d_4 by 3 μl aliquots. The molar ratio of detergent to spin-label was 60:1. The maximal amount of deuterated methanol in the sample was 3 μl. The pH of the samples was controlled before and after addition of the spin probe. For all NMR experiments 5 mm NMR tubes (WILMAD Glass Co., Inc.) were used.

NMR spectroscopy

All NMR spectra (NOESY, TOCSY, DQF-COSY, ROESY) were measured with a Varian Unity-600 spectrometer equipped with triple resonance probe, actively shielded z-gradient coil and a current amplifier PERFOR-

MA II. The WATERGATE[42] scheme was used for water signal suppression. The water-protein cross-peaks in ROESY spectra were narrowed by suppressing radiation dumping in evolution and mixing times, using a weak (50 mG/cm) gradient of magnetic field[43]. The processing of time-domain NMR data was performed with a VNMR program, Varian software, as described[30]. For the diffusion measurements a slightly modified version of the spin echo experiment[44] was used. Before the diffusion experiments started the temperature of the sample (30 °C) was allowed to equilibrate for at least one hour. The calibration of the gradient unit was performed using the same method and the set of solvents.[45] A set of 30 one-dimensional experiments were recorded with the strength of the encoding/decoding pulse field gradients being varied in the range from 0 to ca. 30 Gs/cm. Delays of 150-350 ms were used for the diffusion. A relaxation delay of five seconds was used prior to each scan. The signals of well-resolved protons in 1D spectra were used for the processing of diffusion data of CTII, CTII/DPC complexes or non-deuterated DPC. Self-diffusion rates and their uncertainties were obtained by the two-parameter least-squares exponential fit to the signal decays *versus* the square of the gradient strength.

The rates of amide protons exchange on deuterons were determined by the exponential fitting of measured cross-peak volumes in the finger-print region of TOCSY spectra measured in a four-hour repetition cycle *versus* time elapsed after dissolution of the CTII/DPC sample in ^2H_2O (pH 5.5) at 30 °C.

The fitting of the CTII proton signal chemical shift dependencies on pH was made according to the following equation for a one-proton titration process:

$$\delta = \frac{\delta_h + \delta_l \times 10^{pK-pH}}{1 + 10^{pK-pH}} \quad (1)$$

where δ represents the current chemical shift and δ with the subscripts l and h are for a state at low pH and a state at high pH, respectively.

CTII spatial structure determination

The analysis of processed NMR spectra and measurement of cross-peak volumes in NOESY spectra were performed with the program XEASY.[46] $^3J_{HN\alpha}$ coupling constants were measured with the routine ''INFIT'' of the XEASY program. $^3J_{\alpha\beta}$ coupling constants were evaluated by the analysis of patterns of α/β cross-peaks in a DQF-COSY spectrum of the CTII/DPC sample in ^2H_2O.

The preparation of distance and angle constraints used as input for DYANA[47] calculations as well as treatment of side-chains in the structure calculation protocol and determination of tightly bound water molecules, were performed as described.[30] For local structure analysis and evaluation of medium and long-range distance constraints 50 and 100 ms NOESY spectra were used, respectively. In calculation with DYANA (version 1.5) the protocol of simulated annealing by molecular dynamics (TAD) was used: 12000 TAD steps were performed for 220 starting structures. The MOLMOL program[48] was used for visualization and structure analysis.

Modeling of CTII/DPC micelle interaction interface and calculation of CTII orientation

The first molecule from the set of 20 best structures of CTII in DPC micelles was provided with a chain of 20 pseudo-residues attached to the C terminus. The terminal 80th residue contained a heavy atom (introduced to facilitate manipulation with the molecule within the MOLMOL program) and was presumed to correspond to a virtual micelle center. The DYANA program was used to position the CTII molecule (all dihedral angles of residues 1-60 were fixed) respective to the surface (concave or convex) of a radius from 20 Å to 300 Å. The selection of the surface was made by the minimum of DYANA target function. The distances from backbone atoms of residues 1-60 to the center of the virtual surface were used as upper and lower distance constraint. These constraints were based on the cross-peak broadening in the finger print region of the TOCSY spectrum of CTII/DPC micelle complexes induced by the 5 and 16-doxylstearate relaxation probes (see above). The upper distance constraints in the model of convex spheres (lower ones for the concave spheres) correspond to distances from NH, H^α protons to a center of the sphere which are less than its radius. The lower distance constraints (upper ones for the model of the concave sphere) correspond to distances exceeding the radius of the sphere. The analysis of the model (determination of CTII atoms buried into the micelle, calculation of the CTII surface embedded into micelle etc.) was made with appropriate routines of the MOLMOL program.[48]

PDB and BMRB accession codes

The chemical shifts of CTII in the presence of DPC micelles have been deposited in BioMagneticResonanceBank (accession code of 4815). NMR constraints and derived atomic coordinates (20 models) have been deposited in the RCSB Protein Data Bank (accession code of 1FFJ).

Acknowledgments

This work was supported by a grant from the Russian Basic Research Foundation (project number 98-04-48527) and grant number 414/98/1DP of the project ''Russia Universities - Basic Researches''. The partial financial support for the project CPR/RUS98-01 from the International Centre for Genetic Engeneering and Biotechnology (ICGEB) is acknowledged. Dr R. Efremov is thanked for stimulating discussion and Yu.A. Kosinsky for subroutines used in the analysis of NMR data.

References

1. Kumar, T. K. S., Jayaraman, G., Lee, C. S., Arunkumar, A. I., Sivaraman, T., Samuel, D. & Yu, C. (1997). Snake venom cardiotoxins-structure, dynamics, function and folding. *J. Biomol. Struct. Dynam.* **15**, 431-463.
2. Lauterwein, J. & Wüthrich, K. (1978). A possible structural basis for the different modes of action of neurotoxins and cardiotoxins from snake venoms. *FEBS Letters,* **93**, 181-184.
3. Endo, T. & Tamiya, N. (1987). Current view on the structure-function relationship of postsynaptic

neurotoxins from snake venoms. *Pharmacol. Ther.* **34**, 403-451.
4. Harvey, A. L. (1985). Cardiotoxins from cobra venoms: possible mechanisms of action. *J. Toxicol. Toxin Rev.* **4**, 41-69.
5. Fletcher, J. E., Hubert, M., Wieland, S. J., Gong, Q.-H. & Jiang, M.-S. (1996). Similarities and differences in mechanisms of cardiotoxins, melittin and other myotoxins. *Toxicon*, **34**, 1301-1311.
6. Vincent, J. P., Schweitz, H., Chicheportische, R., Fosset, M., Balerna, M., Lenoir, M. C. & Lazdunski, M. (1976). Molecular mechanism of cardiotoxin action on axonal membranes. *Biochemistry*, **15**, 3171-3175.
7. Dufourcq, J. & Faucon, J. P. (1978). Specific binding of a cardiotoxin from *Naja mossambica mossambica* to charged phospholipids detected by intrinsic fluorescence. *Biochemistry,* **17**, 1170-1176.
8. Dempsey, C. E. (1990). The actions of melittin on membranes. *Biochim. Biophys. Acta,* **1031**, 143-161.
9. Aripov, T. F., Rozenstein, I. A., Salakutdinov, B. A., Lev, A. A. & Gotlib, V. A. (1987). The influence of cytotoxins from central asian cobra venom and melittin from bee venom on the thermodynamic properties of phospholipid bilayer. *Gen. Physiol. Biohys.* **6**, 343-357.
10. Carbone, M. A. & Macdonald, P. M. (1996). Cardiotoxin II segregates phosphatidylglycerol from mixtures with phosphatidylcholione: ^{31}P and ^{2}H NMR spectroscopic evidence. *Biochemistry,* **35**, 3368-3378.
11. Picard, F., Pézolet, M., Bougis, P. E. & Auger, M. (1996). Model of interaction between a cardiotoxin and dimyristoylphosphatidic acid bilayers determined by solid-state ^{31}P NMR spectroscopy. *Biophys. J.* **70**, 1737-1744.
12. Batenburg, A. M., Bougis, P. E., Rochat, H., Verkleij, A. J. & de Kruijff, B. (1985). Penetration of a cardiotoxin into cardiolipin model membranes and its implication on lipid organization. *Biochemistry,* **24**, 7101-7110.
13. Chien, K. Y., Huang, W. N., Jean, J. H. & Wu, W. G. (1991). Fusion of sphingomyelin vesicles induced by proteins from Taiwan cobra (*Naja naja atra*) venom. Interactions of zwitterionic phospholipids with cardiotoxin analogues. *J. Biol. Chem.* **266**, 3252-3259.
14. Aripov, T. F., Gasanov, S. E., Salakhutdinov, B. A., Rozenstein, I. A. & Kamaev, F. G. (1989). Central asian cobra venom cytotoxins-induced aggregation, permeability and fusion of liposomes. *Gen. Physiol. Biophys.* **8**, 459-474.
15. Bougis, P., Tessier, M., Van Rietschoten, J., Rochat, H., Faucon, J. F. & Dufourcq, J. (1983). Are interactions with phospholipids responsible for pharmacological activities of cardiotoxins? *Mol. Cell Biochem.* **55**, 49-64.
16. Chien, K.-Y., Chiang, C.-M., Hseu, Y.-C., Vyas, A. A., Rule, G. S. & Wu, W. (1994). Two distinct types of cardiotoxin as revealed by the structure and activity relationship of their interaction with zwitterionic phosholipid dispersions. *J. Biol. Chem.* **269**, 14473-14483.
17. Jayaraman, G., Kumar, T. K. S., Tsai, C.-C., Srisailam, S., Chou, S.-H. & Ho, C.-L. (2000). Elucidation of the solution structure of cardiotoxin analogue V from the Taiwan cobra (*Naja naja atra*) - identification of structural features important for the lethal action of snake venom cardiotoxins. *Protein Sci,* **9**, 637-646.
18. Ksenzhek, O. S., Gevod, V. S., Omel'chenko, A. M., Semenov, S. N., Sotnichenko, A. I. & Miroshnikov, A. I. (1978). Interaction of the cardiotoxin from the venom of the cobra *Naja naja oxiana* with phospholipid membrane model system. *Molekulyarnaya Biologiya,* **12**, 1057-1065.
19. Gilquin, B., Roumestand, C., Zinn-Justin, S., Ménez, A. & Toma, F. (1993). Refined three-dimensional solution structure of a snake cardiotoxin: analysis of the side-chain organization suggests the existence of a possible phospholipid binding site. *Biopolymers,* **33**, 1659-1675.
20. Golovanov, A. P., Efremov, R. G., Jaravine, V. A., Vergoten, G. & Arseniev, A. S. (1995). Amino acid residue: is it structural or functional? *FEBS Letters,* **375**, 162-166.
21. Surewicz, W. K., Stepanik, T. M., Szabo, A. G. & Mantsch, H. H. (1988). Lipid-induced changes in the secondary structure of snake venom cardiotoxins. *J. Biol. Chem.* **263**, 786-790.
22. Dufourcq, J., Faucon, J. F., Bernard, E., Pézolet, M., Tessier, M. & Bougis, P., *et al.* (1982). Structure-function relationships for cardiotoxins interacting with phospholipids. *Toxicon,* **20**, 165-174.
23. Pézolet, M., Duchesneau, L., Bougis, P., Faucon, J. F. & Dufourcq, J. (1982). Conformation of free and phospholipid-bound cardiotoxins from *Naja mosambicca mosambicca* by laser Raman spectroscopy. *Biochim. Biophys. Acta,*, **704**, 515-523.
24. Sun, Y.-J., Wu, W., Chiang, C.-M., Hsin, Y.-A. & Hsiao, C.-D. (1997). Crystal structure of cardiotoxin V from Taiwan cobra venom: pH-dependent conformational change and a novel membrane-binding motif identified in the three-finger loops of P-type cardiotoxin. *Biochemistry,* **36**, 2403-2413.
25. Sue, S.-C., Rajan, P. K., Chen, T.-S., Hsieh, C.-H. & Wu, W. (1997). Action of Taiwan cobra cardiotoxin on membranes: binding modes of a β-sheet polypeptide with phosphatidylcholine bilayers. *Biochemistry,* **36**, 9826-9836.
26. Bilwes, A., Rees, B., Moras, D., Menez, R. & Ménez, A. (1994). X-ray structure at 1. 55 Å of toxin gamma, a cardiotoxin from *Naja nigricollis* venom. Crystal packing reveals a model for insertion into membranes. *J. Mol. Biol.* **239**, 122-136.
27. Pervushin, K. V. & Arseniev, A. S. (1995). NMR spectroscopy in the study of the spatial structure of membrane peptides and proteins. *Bioorg. Khim.* **21**, 83-111.
28. Dauplais, M., Neumann, J. M., Pinkasfeld, S., Ménez, A. & Roumestand, C. (1995). An NMR study of the interaction of cardiotoxin γ from *Naja nigricollis* with perdeuterated dodecylphosphocholine micelles. *Eur. J. Biochem.* **230**, 213-220.
29. Chiang, C. M., Chien, K. Y., Lin, H. J., Lin, J. F., Yeh, H. C., Ho, P. L. & Wu, W. G. (1996). Conformational change and inactivation of membrane phospholipid-related activity of cardiotoxin V from Taiwan cobra venom at acidic pH. *Biochemistry,* **35**, 9167-9176.
30. Dementieva, D. V., Bocharov, E. V. & Arseniev, A. S. (1999). Two forms of cytotoxin II (cardiotoxin) from *Naja naja oxiana* in aqueous solution. Spatial structures with tightly bound water molecules. *Eur. J. Biochem.* **263**, 152-162.
31. Bechinger, B. (1996). Towards membrane protein design: pH-sensitive topology of histidine-containing polypeptides. *J. Mol. Biol.* **263**, 768-775.

32. Dementieva, D. V., Utkin, Yu. N. & Arseniev, A. S. (1996). Secondary structure and conformational heterogeneity of cytotoxin II from *Naja naja oxiana*. *Bioorg. Khim.* **22**, 289-302.
33. Brown, L. R., Bösch, C. & Wüthrich, K. (1981). Location and orientation relative to the micelle surface for glucagon in mixed micelles with dodecylphosphocholine: EPR and NMR studies. *Biochim. Biophys. Acta,* **642**, 296-312.
34. Brown, L. R., Braun, W., Kumar, A. & Wüthrich, K. (1982). High resolution nuclear magnetic resonance studies of the conformation and orientation of melittin bound to a lipid-water interface. *Biophys. J.* **37**, 319-328.
35. Franklin, J. C., Ellena, J. F., Jayasinghe, S., Kelsh, L. P. & Cafiso, D. S. (1994). Structure of micelle-associated alamethicin from ^{1}H NMR. Evidence for conformational heterogeneity in a voltage-gated peptide. *Biochemistry,* **33**, 4036-4045.
36. Papavoine, C. H., Konings, R. N., Hilbers, C. W. & van de Ven, F. J. (1994). Location of M13 coat protein in sodium dodecyl sulfate micelles as determined by NMR. *Biochemistry,* **33**, 12990-12997.
37. Lauterwein, J., Bösch, C., Brown, L. R. & Wüthrich, K. (1979). Physicochemical studies of the protein-lipid interactions in melittin-containing micelles. *Biochim. Biophys. Acta,* **556**, 244-264.
38. Segrest, J. P., Deloof, H., Dohlman, J. G., Brouillette, C. G. & Anantharamaiah, G. M. (1990). Amphipathic helix motif - classes and properties. *Proteins: Struct. Funct. Genet.* **8**, 103-117.
39. de Planque, M. R. R., Kruijtzer, J. A., Liskamp, R. M., Marsh, D., Greathouse, D. V., Koeppe, R. E., II, de Kruijff, B. & Killian, J. A. (1999). Different membrane anchoring positions of tryptophan and lysine in synthetic transmembrane alpha-helical peptides. *J. Biol. Chem.* **274**, 20839-20846.
40. Hristova, K., Wimley, W. C., Mishra, V. K., Anantharamiah, G. M., Segrest, J. P. & White, S. H. (1999). An amphipathic α-helix at a membrane interface: a structural study using a novel X-ray diffraction method. *J. Mol. Biol.* **290**, 99-117.
41. Brown, L. R. (1979). Use of fully deuterated micelles for conformational studies of membrane proteins by high resolution ^{1}H nuclear magnetic resonance. *Biochim. Biophys. Acta,* **557**, 135-148.
42. Piotto, M., Saudek, V. & Sklenář, V. (1992). Gradient tailored excitation for single-quantum NMR spectroscopy of aqueous solutions. *J. Biomol. NMR,* **2**, 661-665.
43. Sklenář, V. (1995). Suppression of radiation dumping in multidimensional NMR experiments using magnetic field gradients. *J. Magn. Reson. sect. A,* **114**, 132-135.
44. Altieri, A. S., Hinton, D. P. & Byrd, R. A. (1995). Asssociation of biomolecular systems *via* pulsed field gradient NMR self-diffusion measurements. *J. Am. Chem. Soc.* **117**, 7566-7567.
45. Orekhov, V. Yu. , Korzhnev, D. M., Pervushin, K. V. & Arseniev, A. S. (1999). Sampling of protein dynamics in nanosecond time scale by 15N NMR relaxation and self-diffusion measurements. *J. Biomol. Struct. Dynam.* **17**, 157-174.
46. Bartels, C., Xia, T., Billeter, M., Güntert, P. & Wütrich, K. (1995). The program XEASY for computer-supported NMR spectral analysis of biological macromolecules. *J. Biomol. NMR,* **6**, 1-10.
47. Güntert, P., Mumenthaler, C. & Wüthrich, K. (1997). Torsion angle dynamics for NMR structure calculation with new program DYANA. *J. Mol. Biol.* **273**, 283-298.
48. Koradi, R., Billiter, M. & Wütrich, K. (1996). MOLMOL: a program for display and analysis of macromolecular structures. *J. Mol. Graph.* **14**, 51-55.

Edited by B. Holland

(Received 2 August 2000; received in revised form 17 October 2000; accepted 23 October 2000)

http://www.academicpress.com/jmb

Supplementary material for this paper is available on IDEAL